Appl. Phys. B 82, 431–437 (2006)
DOI: 10.1007/s00340-005-2022-z

Applied Physics B
Lasers and Optics

M.C. LARCIPRETE[1,✉]
D. HAERTLE[2]
A. BELARDINI[1,3]
M. BERTOLOTTI[1]
F. SARTO[4]
P. GÜNTER[2]

Characterization of second and third order optical nonlinearities of ZnO sputtered films

[1] INFM at Università di Roma "La Sapienza", Dipartimento di Energetica, Via A. Scarpa, 16-00161 Rome, Italy
[2] Nonlinear Optics Laboratory, Institute of Quantum Electronics, ETH Hönggerberg, 8093 Zürich, Switzerland
[3] Rome, Italy and Università di Roma Tre – Dipartimento di Fisica, Rome, Italy
[4] ENEA, Division of Advanced Physics Technologies, Via Anguillarese, 301-00060 Rome, Italy

Received: 29 July 2005/Revised version: 7 September 2005
Published online: 1 December 2005 •

ABSTRACT We measured the second and third order optical nonlinearity of zinc oxide, grown on glass substrates by the ion beam sputtering technique. Second and third harmonic generation measurements were performed by means of the rotational Maker fringes technique for different polarization configurations, thus allowing the determination of all non-zero components of the second order susceptibility at three different fundamental beam wavelengths, i.e., 1064 nm, 1542 nm and 1907 nm. The dispersion of the nonlinear optical coefficients has been evaluated, while the nonlinear optical coefficients were found to range between 0.9 pm/V and 0.16 pm/V for d_{33}, 0.53 pm/V and 0.08 pm/V for $|d_{15}|$, 0.31 and 0.08 pm/V for $|d_{31}|$, with increasing wavelength. Finally, one third order susceptibility, $\chi^{(3)}_{ijkl}$, has been determined by third harmonic generation measurements at a fundamental wavelength $\lambda = 1907$ nm and a value for $\chi^{(3)}_{3333}$ of 185×10^{-20} m^2/V^2 has been found.

PACS 42.65.An; 42.65.Ky; 42.70.Nq

1 Introduction

Zinc oxide (ZnO) is a II–VI semiconductor with a hexagonal wurtzite crystal structure, like GaN and AlN [1]. Owing to its wide ($E_g = 3.37$ eV) direct band-gap [2], it offers great potential for the fabrication of optoelectronic devices. Recent years have witnessed increased interest in this transparent oxide for a wide range of applications due to its interesting properties. When doped with aluminum, it shows low electrical resistance [3, 4] combined with high optical transmittance in the visible and near infrared range, thus being competitive with indium tin oxide for application as a transparent electrode [5]. Concerning its nonlinear optical properties, it shows second [6–9] and third [10, 11] order optical nonlinear behavior, both in crystals and thin films. Therefore it is a suitable material for the realization of nonlinear optical devices. Nowadays ZnO films are grown by several different deposition techniques, each one of them presenting its peculiarities. These methods include radio frequency sputtering (rf) [12], molecular beam epitaxy [13], pulsed laser deposition [14], just to name some. As a consequence of different crystallinity in these samples, both linear and nonlinear optical properties are generally influenced by the employed technique. Second order nonlinear optical response has been shown in ZnO films grown by laser deposition [6], reactive sputtering [7] as well as spray pyrolysis [8]. Third harmonic generation as well was recently observed in ZnO nanocrystalline films [15]. The possibility to get a nonlinear optical response in thin films is particularly attractive, especially since they can be easily used for integrated nonlinear optical devices.

In second harmonic generation (SHG) experiments the frequency of the incoming beam, ω, is doubled by the second order optical susceptibility $\chi^{(2)}_{ijk}(-2\omega, \omega, \omega)$ of the nonlinear material. Consequently, the components of the third rank tensor $\chi^{(2)}_{ijk}$ can be determined with reference to a well-characterized sample, which in our case is α-quartz. These SHG processes are strongly dependent on the crystalline structure of the material. In particular, SHG can be obtained only in materials which are noncentrosymmetric.

On the other hand, third harmonic generation (THG) is responsible for the frequency tripling of the incoming beam at ω, via the third order susceptibility, $\chi^{(3)}_{ijkl}(-3\omega, \omega, \omega, \omega)$ which is symmetry-allowed in all materials. As a result, from the Maker fringes [16] of the generated signal at 3ω, the components of the fourth rank tensor $\chi^{(3)}_{ijkl}$, can also be evaluated.

In this work, we characterize the second and third nonlinear optical properties of zinc oxide films grown by dual ion beam sputtering technique [17]. ZnO bulk crystal structure, i.e., wurtzite, has the noncentrosymmetric point group symmetry 6 mm with a hexagonal primary cell. Its nonvanishing second order susceptibility tensor elements [18] are $\chi^{(2)}_{311} = \chi^{(2)}_{322}, \chi^{(2)}_{333}$, and $\chi^{(2)}_{113} = \chi^{(2)}_{131} = \chi^{(2)}_{223} = \chi^{(2)}_{232}$ which, using Kleinmann symmetry without dispersion [19], reduce to only three coefficients. Furthermore, an abbreviated notation is usually adopted to replace the last two subscripts of $\chi^{(2)}_{ijk}$ by a single subscript running from 1 to 6 according to the piezoelectric contraction [20]. Unless differently addressed, in what follows this notation will be followed, thus the three nonvanishing coefficients for ZnO become $\chi^{(2)}_{31}$ $\chi^{(2)}_{15}$ and $\chi^{(2)}_{33}$. On the other hand, the third order susceptibility has only two nonvanishing tensor elements [21]: $\chi^{(3)}_{1111}$ and $\chi^{(3)}_{3333}$. However, since in our samples the optical axis is normal to the sample surface, it is possible to address only the component $\chi^{(3)}_{3333}$.

✉ Fax: +39 06 44240183,
E-mail: mariacristina.larciprete@uniroma1.it

SHG and THG measurements were carried out by means of the rotational Maker fringes technique [22] working in the transmission scheme. A quartz plate has been used as a reference. The dispersion of the second order nonlinear optical tensor for ZnO has been investigated for three different fundamental wavelengths using light from a Nd:YAG laser and a Raman shifting cell, i.e., 1064 nm, 1542 nm and 1907 nm. Likewise, measurements of THG were performed at the fundamental wavelength 1907 nm, in order to determine $\chi^{(3)}_{3333}$.

After giving short details on the deposition technique, we describe the experimental setup adopted for the SHG and THG measurements. Finally, the theoretical model for the analysis of the experimental data is illustrated and the obtained values for both second and third order nonlinearity are given. Moreover preliminary deductions on the crystalline structure of the ZnO films are discussed, based on our nonlinear optical measurements.

2 ZnO grown by dual ion beam sputtering

Since most crystal growth techniques are in general expensive and time-consuming, films are meeting increasing interest due to better cost efficiency. On the other hand, films are polycrystalline, and, therefore, show lower optical nonlinearities as compared to crystals. Nevertheless, the film deposition techniques are usually cheaper, faster and, furthermore, also allow the possibility to grow multilayer structures. Following these considerations, it is evidently interesting to explore the ability offered by the film deposition technique by characterizing the nonlinear optical response of the produced films.

Zinc oxide films were deposited by means of a dual ion beam sputtering (DIBS) system [23]. Briefly, DIBS is an established technique for thin film deposition due to the wide range of deposition conditions it offers. Moreover, the low substrate temperature during deposition helps minimizing thermal stress at the film/substrate interface. As a result, this technique can be used for layer deposition on both glass and polymeric substrates, thus offering some advantages with respect to more conventional rf sputtering. The deposition was carried out under vacuum, the chamber being evacuated by a turbo molecular pump to a final pressure of approximately 10^{-10} bar. The working pressure was then kept at a constant value of 10^{-8} bar by controlling the ion source gases. Films were deposited onto 1 mm thick silica substrates, which were previously chemically cleaned in order to remove dust and organic contaminants by washing them in ethylic alcohol and, thereafter, by exposing them to dry air flux. Concerning the temperature, at the beginning of deposition the substrate was at ambient temperature (27 °C), while afterwards its temperature rose by about 10 °C. The energy of the sputtering ion beam was set to be 1200 eV while the ion current, measured at the grid aperture, was set to 20 mA. Under these deposition conditions, the growth rate was found to be 1.1 Å/s. After deposition, the film thickness was measured with a standard profilometer (Alpha-Tencor).

In a previous work [24], we have performed X-ray diffraction (XRD) investigations on similar samples in order to retrieve information on the crystalline structure of the samples. The obtained XRD profiles show that the films are polycrystalline with the *c*-axis preferentially oriented perpendicularly to the film surface [25].

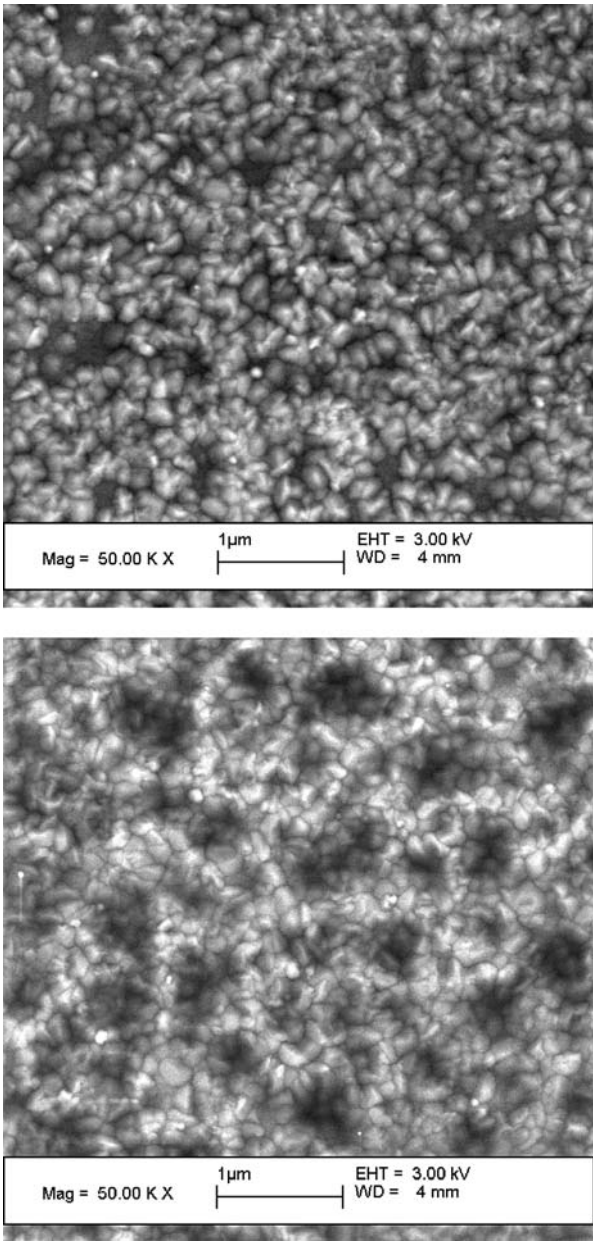

FIGURE 1 SEM images of the investigated zinc oxide films, grown by ion beam sputtering

Furthermore, the morphology of as-grown films was assessed using scanning electron microscope (SEM). As expected, the SEM micrographies, shown in Fig. 1, revealed a polycrystalline structure, with the zinc oxide grains well observable and roughly hexagonal in shape. The average size of the crystal grains can be evaluated to be ~ 150 nm.

3 Experimental setup

The schematic representation of the experimental setup is shown in Fig. 2. As a fundamental beam we used the output of a Q-switched Nd:YAG laser ($\lambda = 1064$ nm, repetition rate in the range 1–14 Hz, 7 ns pulse width). The wave-

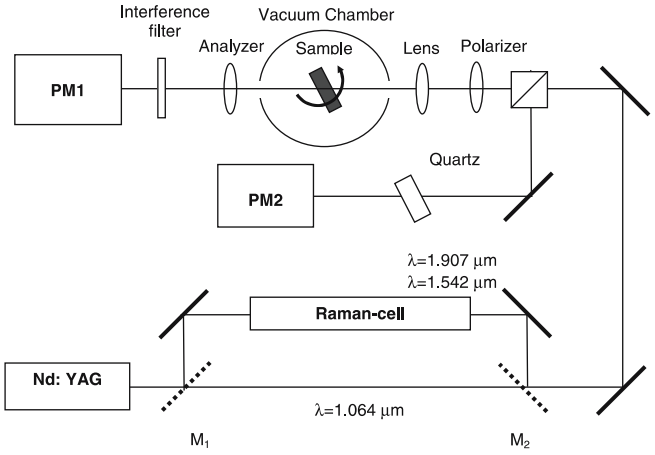

FIGURE 2 Experimental setup for second harmonic generation measurements. M_1 and M_2 are flappable mirrors allowing to send the beam either through the Raman cell or not

length of the fundamental beam could be shifted to 1542 and 1907 nm by means of a Raman cell filled with CH_4 and H_2, respectively. In order to minimize the influence of laser energy fluctuations, a fraction of the fundamental beam was split to the reference line of the setup, where the SH signal from a quartz plate was simultaneously measured at a fixed angle. On the measurement line, the main beam was focused onto the sample with lens of a 500-mm focal length. A motorized rotation stage allowed the variation of the incidence angle, with a resolution of 0.01 degrees. The directions of fundamental and generated beam polarization states were selected by rotating a half-wave plate and a linear analyzer, respectively. After passing the sample, the residual part of the fundamental beam was removed by means of dichroic filters for $\lambda = 1064$ nm, while a cuvette filled with water was used to absorb the Raman-shifted fundamental wavelengths. The second harmonic signal was measured by means of a photomultiplier whose output was then fed into a box-car averager, thus increasing the signal-to-noise ratio. During the reference measurements, detector saturation was prevented using linear neutral density filters, whose transmittance value was taken into account during data fitting. Finally, the data were sent to a computer which was also controlling the experiment. The zinc oxide measurements were referenced against a well known nonlinear optical material, α quartz, characterized by a $\chi^{(2)}_{11}$ ranging from 0.60 pm/V (at $\lambda = 1064$ nm) to 0.56 pm/V (at $\lambda = 1907$ nm) [16]. Considering the polarization states, if we refer to the fundamental and generated beams by means of the subscripts ω and 2ω, the reference quartz was measured in $p_\omega p_{2\omega}$, $45_\omega p_{2\omega}$ and $s_\omega s_{2\omega}$ configuration, while ZnO was measured in $p_\omega p_{2\omega}$, $45_\omega p_{2\omega}$ and $s_\omega p_{2\omega}$, respectively. From the experimental point of view, a critical point is represented by the decreasing amplitude of the generated signal, when the polarization of fundamental beam is rotated from p_ω, giving the highest signal, to s_ω, giving the lowest one. Furthermore, due to dispersion of the second order nonlinear optical coefficients the generated signal decreases for an increasing fundamental wavelength.

Additional third harmonic generation (THG) measurements were performed under the same experimental conditions, the only difference being that the sample was kept under vacuum during experiments. Concerning the magnitude of the third harmonic signal, it is worth to note that when dealing with THG phenomena, the linear absorption of the material plays an important role, since the generated signal at 3ω may fall within the absorption band. Contrarily, the wavelength dispersion of the nonlinearity suggests the use of a fundamental beam at lower wavelength to get strong signals. As a consequence, in our experiments, we could only succeed getting the measurements of the third harmonic signal when the fundamental beam is 1907 nm and, therefore, characterized $\chi^{(3)}_{3333}$ at this wavelength.

4 Second harmonic generation: theory and measurements

The expression of the SH power $W_{2\omega}$, as a function of incidence angle α, is given by [20]:

$$W_{2\omega}(\alpha) = \left(\frac{512\pi^3}{A}\right) t^4_\omega(\alpha) T_{2\omega}(\alpha) W^2_\omega \frac{sin^2\left(\Psi_{\mathrm{SHG}}(\alpha)\right)}{[n^2_\omega(\alpha) - n^2_{2\omega}(\alpha)]^2} d^2_{\mathrm{eff}}(\alpha) \quad (1)$$

where A is the fundamental beam transverse area, W_ω is the power of the incident fundamental beam, t_ω is the fundamental field transmission coefficient at the input interface, $T_{2\omega}$ is the SH power transmission coefficient at the output interface (Fresnel coefficients), n_ω and $n_{2\omega}$ are the refractive indices at the fundamental and generated frequency [19]. The transverse profile of the fundamental beam has been assumed to be uniform. From the structure of the measured Maker fringes, one can determine the coherence length,

$$l_c = \frac{\pi}{k_{2\omega} - 2k_\omega} = \frac{\pi c}{2\omega |n_\omega(\alpha)\cos(\alpha'_\omega) - n_{2\omega}(\alpha)\cos(\alpha'_{2\omega})|}.$$

Finally, $\Psi_{\mathrm{SHG}}(\alpha)$ is a phase factor given by:

$$\Psi_{\mathrm{SHG}} = \left(\frac{\pi L}{2}\right)\left(\frac{4}{\lambda}\right)\left[n_\omega(\alpha)\cos(\alpha'_\omega) - n_{2\omega}(\alpha)\cos(\alpha'_{2\omega})\right] \quad (2)$$

where L is sample thickness, α'_ω and $\alpha'_{2\omega}$ the propagation angles in the material corresponding to ω and 2ω, which are given by Snell's law by $\sin\alpha = n_\omega \sin\alpha'_\omega$ (and $\sin\alpha = n_{2\omega}\sin\alpha'_{2\omega}$). Particular attention must be given to the term $d_{\mathrm{eff}}(\alpha)$ which represents the effective susceptibility. The analytical expression of $d_{\mathrm{eff}}(\alpha)$ can be rather complicated [26], being dependent on the $d_{ijk} = \frac{1}{2}\chi^{(2)}_{ijk}$ tensor components, the polarization of both first and second harmonic electric fields and, of course, on the fundamental beam incidence angle, α. However, it can be significantly simplified for particular crystalline symmetries. Specifically, given that $\chi^{(2)}_{ijk}$ for ZnO only has three nonzero-components [27], the final expressions for $d_{\mathrm{eff}}(\alpha)$ at the different polarization configurations in the abbreviated notation are:

$$\begin{aligned} d^{s_\omega p_{2\omega}}_{\mathrm{eff}} &= d_{31}\sin\alpha_{2\omega} \\ d^{45_\omega p_{2\omega}}_{\mathrm{eff}} &= d_{15}\sin\alpha_\omega \\ d^{p_\omega p_{2\omega}}_{\mathrm{eff}} &= d_{15}\cos\alpha_{2\omega}\sin 2\alpha_\omega + d_{31}\cos^2\alpha_\omega \sin\alpha_{2\omega} \\ &\quad + d_{33}\sin^2\alpha_\omega \sin\alpha_{2\omega} \end{aligned} \quad (3)$$

where the apices s_ω-$p_{2\omega}$, 45_ω-$p_{2\omega}$ and p_ω-$p_{2\omega}$ refer to the three different polarization combinations of fundamental and

generated beams. Equation (3) shows that the term d_{31} can be independently evaluated from the measurement of the p-polarized SH signal for a s-polarized fundamental beam; d_{15} from data corresponding to p-polarized SH signal for a 45°-linearly polarized fundamental beam. Finally, the largest component, d_{33}, is addressed when both SH and fundamental beams are p-polarized. It is worth noting that the expression of d_{eff} in the latter case also includes a dependence on d_{31} and d_{15} which can be determined separately. As an additional simplification, when dealing with crystals, Kleinman's symmetry rules can be applied to further reduce the independent components. The wurtzite crystalline structure, in fact, presents internal relations between structural parameters, and to a first approximation allows the assumption $d_{31} \approx d_{15}$ and $|d_{33}| = 2d_{31}$. As a consequence, when the sample is supposed to be crystalline, it is possible to limit the investigation to the measurements of the largest component, i.e., d_{33}, by fitting only of p_ω-$p_{2\omega}$ measurements, which also give the highest signal. Nevertheless, an independent evaluation of the three components, or at least two of them, allows one to get information of the crystallites' main orientation. Here, the nonlinear tensor components, d_{31}, d_{15} and d_{33} have been determined independently for fundamental at $\lambda = 1064$ nm and $\lambda = 1543$, while for $\lambda = 1907$ nm Kleinman's approximation has been taken into account.

To interpolate the SHG experimental curves according to (1) and (2), the fundamental beam power term, W_ω, was calculated from the calibration measurements on quartz. The parameters which are necessary are then reduced to the sample thickness ($L = 550$ nm) and the linear refractive indices values at fundamental, n_ω and generated wavelengths, i.e., $n_{2\omega}$ and $n_{3\omega}$ for SHG and THG, and for the corresponding polarization state. Dispersion of both the ordinary and extraordinary refractive indices of ZnO, $n(\lambda)$, is reported in Table 1 [2].

In Fig. 3 the experimental results for three different measurements of SHG at $\lambda = 1064$ nm are shown, together with the fitting curves. It can be seen that the signal reduces to zero at normal incidence, for all polarization states of the fundamental beam. According to SH theory, this circumstance allows the assumption that the average orientation of the optical axis is normal to the film surface. This effect confirms that the crystalline grains are preferentially oriented along the c-axis.

From the fit of the experimental curves we got the values of nonlinear tensor components, measured at the different wavelengths, which are shown in Table 2. For the fundamental wavelength 1064 nm, $d_{33} = 0.9 \pm 0.09$ pm/V, $|d_{15}| = 0.53 \pm 0.05$ pm/V and $|d_{31}| = 0.31 \pm 0.03$ are the largest obtained values. At the fundamental wavelength 1543 nm, the susceptibility components are $d_{33} = 0.25 \pm 0.02$ pm/V, $|d_{15}| = 0.14 \pm 0.01$ and $|d_{31}| = 0.10 \pm 0.01$ pm/V, and are further reduced

Direction	E_{d} [eV]	E_0 [eV]	E_{d}/E_0
O	16.51	6.20	2.66
E	16.52	6.08	2.71

TABLE 1 Ordinary and extraordinary refractive index dispersion laws for ZnO. The data, reported from [2], have been fitted according to the Sellmeier model with a single oscillator [1]: $(n^2(\lambda) - 1) = E_{\text{d}}E_0/(E_0^2 - E^2)$, being E_0 the single oscillator energy, E_d the dispersion energy and $E = hc/\lambda$

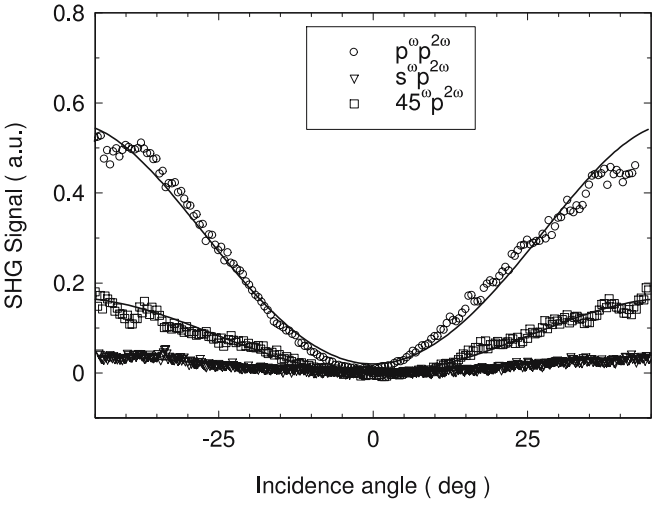

FIGURE 3 Second harmonic signal versus the incidence angle, for three different polarizations of the fundamental beam, while the generated beam is always p-polarized. The fundamental beam wavelength is 1064 nm. Experimental results for $p^\omega p^{2\omega}$ (○), $45^\omega p^{2\omega}$ (□) and $s^\omega p^{2\omega}$ (∇) and corresponding fitting curves (*solid lines*)

Fundamental Wavelength [nm]	$\lvert d_{33}\rvert$ [pm/V]	$\lvert d_{15}\rvert$ [pm/V]	$\lvert d_{31}\rvert$ [pm/V]
1064	0.90±0.09	0.53±0.05	0.31±0.03
1542	0.25±0.02	0.14±0.01	0.10±0.01
1907	0.16±0.02	0.08±0.02	0.08±0.02

TABLE 2 Second order nonlinear optical coefficients of ZnO deposited by dual ion beam sputtering, for different fundamental beam wavelengths

to $d_{33} = 0.16 \pm 0.02$ pm/V, $|d_{31}| = |d_{15}| \sim 0.08 \pm 0.02$ pm/V for a fundamental beam at1907 nm. When d_{31} and d_{15} could be determined each from one independent measurement, the resulting experimental errors of these two coefficients was smaller than that of d_{33}. In Fig. 4 the measured tensor components are reported versus fundamental beam wavelength. The experimental data are represented together with a dotted line which has the function of guide for eyes.

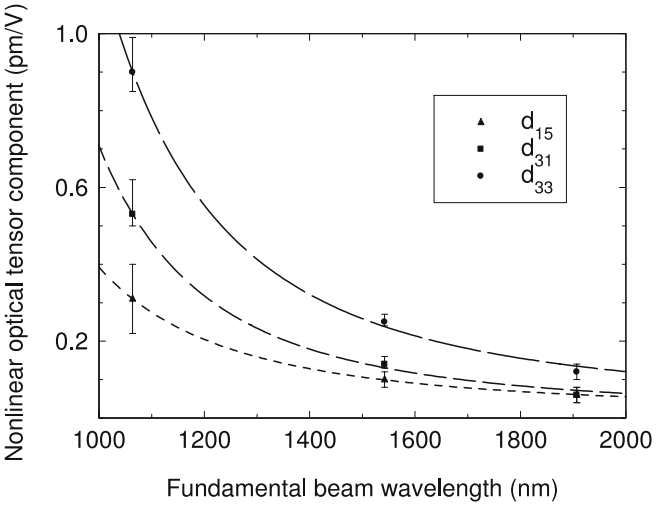

FIGURE 4 Measured nonlinear optical coefficients, d_{33}, d_{31} and d_{15} versus fundamental beam wavelength. *Dashed lines* are included as a guide for eyes

As expected from the theory, the nonlinear optical response shows that d_{33} is always the largest component. From the ratios between the largest component and the others, i.e., d_{33}/d_{15} and d_{33}/d_{31} respectively, it is also possible to get some information on the crystalline structure of the film. For the ideal wurtzite structure, in fact, these two ratios should be equal to 2, while here we found $d_{33}/d_{15} = 1.69$ and 1.78 and $d_{33}/d_{31} = 2.9$ and 2.5. Within the experimental error, the ratios are almost constant for the two measured fundamental wavelengths, 1064 and 1542 nm. This is a further evidence of the necessity of measuring the three different components independently, especially when dealing with polycrystalline structures.

When considering the wavelength dependence of the second order susceptibility, an empirical rule due to Miller [28] can be a useful tool to evaluate the effect of partial crystallinity of the investigated films. Despite its several limits [29, 30] it allows the following expression of the second order susceptibility, $\chi^{(2)}_{ijk}$ or $d_{ijk} = \frac{1}{2}\chi^{(2)}_{ijk}$, in terms of the linear optical susceptibilities at the involved wavelengths. In full subscripts notation:

$$\chi^{(2)}_{ijk}(\omega_1+\omega_2, \omega_1, \omega_2) = \varepsilon_0 \delta_{ijk} \chi^{(1)}_{ii}(\omega_1+\omega_2)\chi^{(1)}_{jj}(\omega_1)\chi^{(1)}_{kk}(\omega_2) \tag{4}$$

where the tensorial subscripts i, j and k, give the direction of polarization for generated and fundamental fields, respectively. It has been noted that for many inorganic materials, the coefficients $\delta_{ijk}(2\omega, \omega, \omega)$, are spread in a range which is much narrower than the changes in d_{ijk} and are almost wavelength independent. It can be, therefore, used to evaluate the magnitude of d_{ijk} over a range of wavelength and, therefore, it is known as Miller's delta. Miller's rule for SHG process, describes accurately the dispersion of second order nonlinear optical susceptibilities for several inorganic materials. When $\omega_1 = \omega_2 = \omega$, and $j = k$, (4) becomes:

$$\chi^{(2)}_{ikk}(2\omega) = \varepsilon_0 \delta_{ikk} \chi^{(1)}_{ii}(2\omega) \left[\chi^{(1)}_{kk}(\omega)\right]^2 . \tag{5}$$

Assuming for ZnO bulk crystal [26] $\delta_{ijk} \sim 7.95 \times 10^{-2}\,\mathrm{m^2/C}$ over the investigated wavelength range, and the dispersion law reported in Table 1, we obtain for the contracted term d_{33} the solid curve which is shown in Fig. 5. It can be seen that the dispersion of the measured nonlinear optical coefficients is consistent with the theory while there is a factor of five between the calculated and measured dispersion curves. The difference in the absolute value is compatible with the observed small grain size of the films, resulting from the low temperature of deposition.

Previously reported measurements show that it is possible to get second harmonic generation from zinc oxide films [6–9]. However, the authors experiencing the highest values used a high temperature deposition technique. In [7], e.g., highly crystalline ZnO films were deposited by reactive pulsed-direct-current sputtering on fused silica and PECVD on sapphire, at a temperature of $\sim 250°$. Samples with thicknesses from 30–350 nm were measured and the nonlinear optical coefficients were found to increase with decreasing thickness, $\chi^{(2)}_{33}$ ranging 6–18 pm/V. In [8], the samples (100–1000 nm thick) were prepared via spray pyrolisis

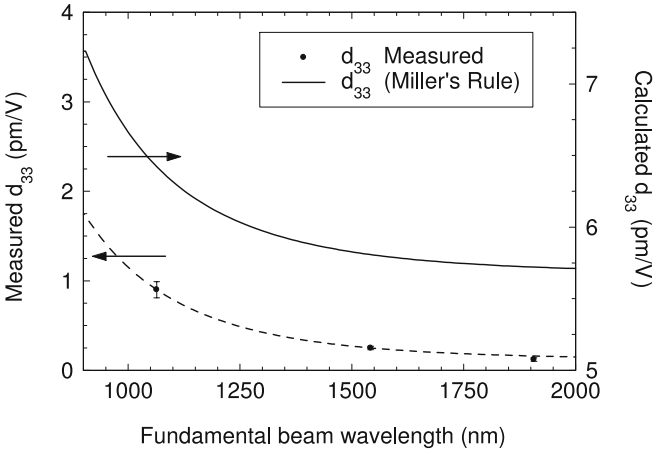

FIGURE 5 Comparison between the measured second order susceptibility d_{33} for a ZnO film prepared by dual ion beam sputtering and the calculated ones for ZnO crystal. The theoretical curve (*solid line*) calculated with the Miller δ

process at 620–870 °K. The values of the nonlinearity were slightly higher than those reported for bulk ($\chi^{(2)}_{31} \sim 4.2$ and $|\chi^{(2)}_{33}| \sim 14.6$ pm/V). In [9] pulsed laser ablation at 500–700° was used to grow samples of different thickness (45–235 nm) and crystallinity (X-ray diffraction peak 0.1–0.7° wide). The highest obtained susceptibility values were $\chi^{(2)}_{31} = 3.6$ pm/V and $\chi^{(2)}_{33} = 13.4$ pm/V. On the other side, when looking specifically for films deposited without a temperature increase, in [6] we found zinc oxide films grown using pulsed laser deposition. In this work thicknesses was varied between 450 and 1050 nm, and the obtained second order nonlinear optical coefficients were similar to those we measured, i.e., $\chi^{(2)}_{31} \sim 0.3$–1 pm/V. These data show that, by keeping room temperature during deposition, as in the case of our technique, second harmonic generation can be obtained, although the values of the second order nonlinearity is of course lower than in bulk material.

5 Third harmonic generation: theory and measurements

We also measured the generated third harmonic signal, within the same experimental setup and, then, characterized the coefficient $\chi^{(3)}_{3333}$ of zinc oxide at $\lambda = 1907$ nm. Different dichroic filters were used to select the spectral radiations at 3ω, thus avoiding the contribution of the SH signal.

The investigated crystal structure presents two components of $\chi^{(3)}_{ijkl}$, namely, $\chi^{(3)}_{1111}$ and $\chi^{(3)}_{3333}$. Being the sample deposited along the (0002) planes, i.e., with the axis mainly normal to sample surface, it was possible to investigate only $\chi^{(3)}_{3333}$ by selecting the $p_\omega p_{3\omega}$ experimental configuration.

Since third order nonlinear optical phenomena are related to an odd powered term in the nonlinear optical polarization [31], third harmonic generation (THG) may occur in any material, including air. It was, therefore, necessary to perform the measurements under vacuum. Air, in fact, may give an important spurious signal at 3ω, since its coherence length for THG, $l_c = \lambda/[6(n^{3\omega} - n^{\omega})]$ at normal incidence, is large due to the weak dispersion in the refractive index.

Furthermore, the investigated material is also non-centrosymmetric, therefore also SHG may take place during THG measurements [32]. Specifically, the generated signal at 3ω via a $\chi^{(3)}(-3\omega, \omega, \omega, \omega)$ process, may include also a contribution from cascaded SHG via a first $\chi^{(2)}(-2\omega, \omega, \omega)$ process and then sum-frequency generation, $\chi^{(2)}(-3\omega, 2\omega, \omega)$. In order to discriminate between the two contributes, it is useful referring to the coherence lengths for the two processes. If, in fact, the coherence length of the latter process, sum-frequency generation (SFG), differs from that of THG, additional fringes appear in the typical Maker fringes curves. This is mainly due to the fact that the coherence length is responsible for the modulation of the signal, see both (1) and (8). Unfortunately, this doesn't hold for zinc oxide since the two coherence lengths are very similar, being:

$$l_c^{\mathrm{THG}} = \frac{\pi}{k_{3\omega} - 3k_{\omega}} = \frac{\lambda}{6\left[n_{3\omega}(\alpha) - n_{\omega}(\alpha)\right]} \cong 4.6\,\mu\mathrm{m} \tag{6}$$

$$l_c^{\mathrm{SFG}} = \frac{\pi}{k_{3\omega} - k_{2\omega} - k_{\omega}} = \frac{\lambda}{6n_{3\omega}(\alpha) - 4n_{2\omega}(\alpha) - 2n_{\omega}(\alpha)} \cong 4.8\,\mu\mathrm{m} \tag{7}$$

Following these considerations, we tried a different method [33] to distinguish among the two processes, i.e., by rotating the sample in the plane of incidence, looking for two configurations where the angle dependence of THG is the same, while it changes for SHG. If any differences are evidenced in the measurements, then they may be ascribed to the sum frequency generation process. Since the wurtzite structure is symmetric on the rotational axis, we did not see any difference when sample are rotated in the incidence plane.

However, it must be pointed out that, even when the cascaded THG through the SHG and the SFG takes place, the efficiency of this process in polycrystalline films is so low that it can be neglected. This assumption is also supported by the relatively small thickness of samples. Furthermore, the investigated polycrystalline samples show a high third order coefficient and a low SHG efficiency, thus we assumed that these effects are negligible.

The full expression for the TH power $W_{3\omega}$, as a function of the incidence angle α, is given by [20]:

$$W_{3\omega}(\alpha) = \left(\frac{2304\pi^6}{A}\right) t_{\omega}^6(\alpha) T_{3\omega}(\alpha) W_{\omega}^3 \frac{\sin^2(\Psi_{\mathrm{THG}}(\alpha))}{\left[n_{\omega}^2(\alpha) - n_{3\omega}^2(\alpha)\right]^2} \left|\chi^{(3)}\right|^2 \tag{8}$$

Here $T_{3\omega}$ is the TH power transmission coefficient at the output interface, n_{ω} and $n_{3\omega}$ are the refractive indices at the fundamental and generated frequency, respectively [34]. Again, $\Psi_{\mathrm{THG}}(\alpha)$ is the phase factor for THG and it is given by:

$$\Psi_{\mathrm{THG}} = \left(\frac{\pi L}{2}\right)\left(\frac{6}{\lambda_{\omega}}\right)\left[n_{\omega}(\alpha)\cos(\alpha'_{\omega}) - n_{3\omega}(\alpha)\cos(\alpha'_{3\omega})\right] \tag{9}$$

In order to calculate the third order nonlinearity, it is necessary to fit the THG experimental measurements according to (8) and (9). As for SHG experiments, once W_{ω} is retrieved from the calibration THG measurements on quartz, the only parameters necessary are sample thickness and the linear dispersion, i.e., n_{ω} and $n_{3\omega}$.

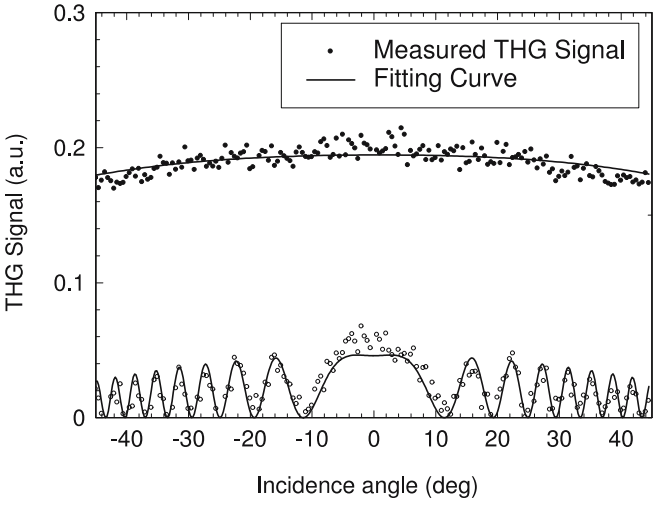

FIGURE 6 Third harmonic signal as a function of incidence angle, for a fundamental beam $\lambda = 1907$ nm. Both generated and fundamental beams are *p*-polarized. Experimental results for the quartz reference sample (○) and for the ZnO film (●) together with the corresponding fitting curves (*solid lines*) are shown. To prevent optical damage the measurements on ZnO were averaged only over 10 light pulses, instead of 30 as for SHG measurements

In Fig. 6 we report a measurement of third harmonic curve at 1907 nm, together with the fitting curve. The Maker fringe experiment at 1907 nm yielded $\chi^{(3)}_{3333} = 185 \times 10^{-20}\,\mathrm{m^2/V^2}$ or 1.32×10^{-12} esu, assuming $\chi^{(3)}_{1111} = 1.99 \times 10^{-22}\ \mathrm{m^2/V^2}$ for quartz. The obtained value is in agreement with those already reported for ZnO films.

6 Conclusions

In conclusion, second and third order nonlinear optical properties of ZnO deposited by dual ion beam sputtering were investigated. SHG was measured at three different wavelengths, and the dispersion of three elements of the second order nonlinearity was derived. As expected, we found that the component d_{33} has always the highest values, ranging from 0.9 ± 0.09 pm/V at 1064 nm to 0.16 ± 0.02 pm/V at 1907 nm, while the other components d_{31} and d_{15} are lower. Considering the absolute values, the investigated film structure shows second order nonlinearity which is five times lower than the corresponding bulk crystal structure. This is a good result when considering the lack of preferential growth direction typical of the DIBS and the low temperature used during deposition. The SHG measurements also confirm that the film has a partially oriented polycrystalline structure, and that the average orientation of the grains optical axis is normal to the input surface. THG experiments were performed at 1907 nm and the measured $\chi^{(3)}_{3333}$ was found to be $185 \times 10^{-20}\,\mathrm{m^2/V^2}$.

From the measured nonlinear optical response, we may conclude that low temperature dual ion beam sputtering technique represents a useful tool to obtain ZnO films with good nonlinear optical characteristics of both second and third order.

ACKNOWLEDGEMENTS S. Paoloni, F. Michelotti and D. Passeri are kindly acknowledged for helpful discussion and interesting comments.

REFERENCES

1 V.A. Karpina, V.I. Lazorenko, C.V. Lashkarev, V.D. Dobrowolski, L.I. Kopylova, V.A. Baturin, S.A. Pustovoytov, A.J. Karpenko, S.A. Eremin, P.M. Lytvyn, V.P. Ovsyannikov, E.A. Mazurenko, Cryst. Res. Technol. **39**, 980 (2004)
2 R. Blachnik, J. Chu, R.R. Galazka, J. Geurts, J. Gutowski, B. Hönerlage, D. Hofmann, J. Kossut, R. Lévy, P. Michler, U. Neukirch, T. Story, D. Strauch, A. Waag, "Zinc oxide (ZnO)" In: Landolt–Börnstein-Group III Condensed Matter, Semiconductors: II–VI and I–VII Compounds; Semi-magnetic Compounds, 41B, 52–53, U. Rössler (Ed.) (Springer-Verlag GmbH, 1999)
3 A. Valentini, F. Quaranta, M. Penza, F.R. Rizzi, J. Appl. Phys. **73**, 1143 (1993)
4 T. Minami, MRS Bulletin **25**, 38 (2000)
5 F. Michelotti, A. Belardini, M.C. Larciprete, M. Bertolotti, A. Rousseau, A. Ratsimihety, G. Shoer, J. Mueller, Appl. Phys. Lett. **83**, 4477 (2003)
6 A. Mitra, R.K. Thareja, Modern Phys. Lett. B **15**, 515 (2001)
7 G. Wang, G.T. Kiehne, G.K. Wong, J.B. Ketterson, X. Liu, R.P.H. Chang, Appl. Phys. Lett. **80**, 401 (2002)
8 U. Neumann, R. Grunwaid, U. Griebner, G. Steinmeyer, W. Seeber, Appl. Phys. Lett. **84**, 170 (2004)
9 H. Cao, J.Y. Wu, H.C. Ong, J.Y. Dai, R.P.H. Chang, Appl. Phys. Lett. **73**, 572 (1998)
10 J.A. Bolger, A.K. Kar, B.S. Wherret, R. De Salvo, D.C. Hutchings, D.J. Hagan, Optics Comm. **97**, 203, 1 (1993)
11 W. Zhang, H. Wang, K.S. Wong, Z.K. Tang, G.K. Wong, R. Jain, Appl. Phys. Lett. **75**, 3321, 2 (1999)
12 Y. Yoshino, K. Inoue, M,Takeuchi, K. Ohwada, Vacuum **51**, 601 (1998)
13 Y.F. Chen, D.M. Bagnall, H.J. Koh, K.T. Park, K. Hiraga, Z. Zhu, T. Yao, J. Appl. Phys. **84**, 3912 (1998)
14 S. Choopun, R.D. Vispute, W. Noch, A. Balsamo, R.P. Sharma, T. Venkatesan, A. Iliadis, D.C. Look, Appl. Phys. Lett. **75**, 3947 (1999)
15 G.I. Petrov, V. Shcheslavskiy, V.V. Yakovlev, I. Ozerov, E. Chelnokov, W. Marine, Appl. Phys. Lett. **83**, 3993 (2003)
16 C. Bosshard, U. Gubler, P. Kaatz, W. Mazerant, U. Meier, Phys. Rev. B **61**, 10 688 (2000)
17 S. Scaglione, G. Emiliani, J. Vac. Sci. Technol. A **3**, 2702 (1985)
18 A. Yariv, Optical Electronics 4th ed. (Saunders College Publishing, USA 1991)
19 P. Günter, *Nonlinear Optical Effects and Materials* (Springer-Verlag, Berlin 2000)
20 V.G. Dmitriev, G.G. Gurzadyan, D.N. Nikogosyan, *Handbook of nonlinear optical crystals* (Springer, Berlin 1997)
21 A. Zappettini, F.D'Amore, S.M. Pietralunga, A. Terio, M. Martinelli, D.F. Bliss, M.J. Callahan, Phys. Stat. Sol. (C) **1**, 997 (2004)
22 J. Jerphagnon, S.K. Kurtz, J. Appl. Phys. **41**, 1667 (1970)
23 F. Sarto, M. Alvisi, E. Melissano, A. Rizzo, S. Scaglione, L. Vasanelli, Thin Solid Films **346**, 196 (1999)
24 M.C. Larciprete, D. Passeri, F. Michelotti, S. Paoloni, C. Sibilia, M. Bertolotti, A. Belardini, F. Sarto, F. Somma, S. Lo Mastro, J. Appl. Phys **97**, 23 501 (2005)
25 K.S. Weißenrieder, J. Muller, Thin Solid Films **300**, 30 (1997)
26 P.A. Franken, J.F. Ward, Rew. Modern Physics **35**, 23 (1963)
27 H.Y. Zhang, X.H. He, Y.H. Shih, M. Schurman, Z.C. Feng, R.A. Stall, Appl. Phys. Lett. **69**, 2953 (1996)
28 R.C. Miller, Appl. Phys. Lett **5**, 17 (1964)
29 S. Scandolo, F. Bassani, Phys. Rev. B **51**, 6928 (1995)
30 P. Gòrski, M. Kin, W. Kucharczyk, J. Phys. D: Appl. Phys. **30**, 1111 (1997)
31 R.W. Boyd, Nonlinear Optics (Academic Press. Inc., Boston 1992)
32 C. Bosshard, R. Spreiter, M. Zgonik, P. Günter, Nonlinear Optics **15**, 425 (1996)
33 G.R. Meredith, Phys. Rev. B **24**, 5522 (1981)
34 U. Gubler, C. Bosshard, Phys. Rev. B **61**, 10 702 (2000)